

ARTICLE

Received 30 Jun 2016 | Accepted 1 Nov 2016 | Published 13 Dec 2016

DOI: 10.1038/ncomms13802

OPEN

Robust spin-orbit torque and spin-galvanic effect at the Fe/GaAs (001) interface at room temperature

L. Chen¹, M. Decker¹, M. Kronseder¹, R. Islinger¹, M. Gmitra², D. Schuh¹, D. Bougeard¹, J. Fabian², D. Weiss¹ & C.H. Back¹

Interfacial spin-orbit torques (SOTs) enable the manipulation of the magnetization through in-plane charge currents, which has drawn increasing attention for spintronic applications. The search for material systems providing efficient SOTs, has been focused on polycrystalline ferromagnetic metal/non-magnetic metal bilayers. In these systems, currents flowing in the non-magnetic layer generate—due to strong spin-orbit interaction—spin currents via the spin Hall effect and induce a torque at the interface to the ferromagnet. Here we report the observation of robust SOT occurring at a single crystalline Fe/GaAs (001) interface at room temperature. We find that the magnitude of the interfacial SOT, caused by the reduced symmetry at the interface, is comparably strong as in ferromagnetic metal/non-magnetic metal systems. The large spin-orbit fields at the interface also enable spin-to-charge current conversion at the interface, known as spin-galvanic effect. The results suggest that single crystalline Fe/GaAs interfaces may enable efficient electrical magnetization manipulation.

¹ Institute of Experimental and Applied Physics, University of Regensburg, 93040 Regensburg, Germany. ² Institute of Theoretical Physics, University of Regensburg, 93040 Regensburg, Germany. Correspondence and requests for materials should be addressed to C.H.B. (email: christian.back@ur.de).

In solids with space-inversion asymmetry intrinsic spin-orbit fields (SOFs) emerge. These SOFs can arise from Dresselhaus spin-orbit interaction (SOI) which originates from bulk inversion asymmetry¹, and/or from Bychkov-Rashba SOI which originates from structure inversion asymmetry². In the limit of small wave vector \mathbf{k} near the Γ point, both SOIs can be expressed by \mathbf{k} -linear terms in the Hamilton operator; that is, $H_D = \beta(\sigma_x k_x - \sigma_y k_y)$ in case of Dresselhaus SOI and $H_R = \alpha(\sigma_x k_y - \sigma_y k_x)$ in case of Bychkov-Rashba SOI. Here $\sigma_{x,y}$ are Pauli spin matrices and α and β characterize the strength of Rashba and Dresselhaus spin-orbit coupling. Figure 1a,b show the SOFs due to Rashba and Dresselhaus SOI. The most striking property of these SOIs is that spin and carrier momentum are coupled, meaning that a charge current is accompanied by a non-equilibrium spin accumulation^{3–5}. The magnitude and orientation of this spin accumulation is controlled by the charge current. It is convenient to quantify this spin accumulation by an effective SOF (eSOF). On the other hand, the inverse process is also applicable: a non-equilibrium spin accumulation drives a charge current⁶. Making use of SOI is thus a promising pathway for future spintronic applications⁷. In fact, it has been demonstrated that SOI can be used to manipulate the magnetization direction by a local current^{8–11}. Thus, establishing a new material system with strong SOI at room temperature is of utmost importance for the realization of practical spin-orbit torque (SOT) devices. Motivated by early work on strained low-temperature (Ga,Mn)As^{10–13}, it has been shown recently that there is sizeable Dresselhaus dominated SOT in the Heusler alloy NiMnSb¹⁴. Furthermore, electric switching in the antiferromagnet CuMnAs by an internal SOT has been demonstrated at room temperature¹⁵.

It is well established that single crystalline Fe thin films grow epitaxially on GaAs (001) due to the small lattice mismatch between twice the lattice constant of Fe (2.87 Å) and GaAs (5.65 Å). The Fe/GaAs interface has C_{2v} symmetry. For this particular interface it has been shown that near the Fermi energy and in the vicinity of the Γ -point the SOFs arising from C_{2v} symmetry can be expressed as a combination of Dresselhaus- and Bychkov-Rashba-like SOFs¹⁶, causing, for example, an anisotropic tunneling magnetoresistance¹⁷ and a crystalline anisotropic magnetoresistance (AMR) with two-fold symmetry, when the Fe layer is only a few monolayers thick¹⁸.

Here we demonstrate that a robust SOT exists at the Fe/GaAs interface at room temperature. We find that the dominating eSOF contribution stems from Bychkov-Rashba-like SOI, and importantly, that the magnitude of the eSOF is comparable to the ones in ferromagnetic metal/non-magnetic metal systems^{19–22}. Moreover, we show that the strong SOI at the interface converts a pure spin current, generated by spin pumping^{23–25}, into a charge current. This is due to the spin-galvanic effect (SGE)⁶ also called inverse Rashba-Edelstein effect²⁶, which is similar to the inverse spin Hall effect (ISHE) in a three dimensional material⁷. Apart from semiconductors it has only been observed at an Ag/Bi interface²⁶ and in the three dimensional Rashba-metal GeTe²⁷. The simple structure of Fe/GaAs used here excludes any bulk contribution via ISHE since the conducting non-magnetic layer is absent. Our results indicate that a single crystalline Fe/GaAs interface is sufficient for electrical magnetization manipulation.

Results

Quantifying eSOFs by spin-orbit ferromagnetic resonance. We determine the strength of the interfacial SOFs by using spin-orbit ferromagnetic resonance (SO-FMR) developed previously to quantify SOFs in the ferromagnetic semiconductor

(Ga,Mn)As^{12,13}. SO-FMR is similar to the spin-torque ferromagnetic resonance (FMR) technique which is used to quantify the spin Hall effect in ferromagnetic metal/non-magnetic metal bilayers⁹. The mechanism is illustrated in Fig. 2a. An alternating in-plane current $j(t)$ flowing in the Fe stripe generates, due to SOI, a time dependent non-equilibrium spin accumulation at the Fe/GaAs interface. This spin accumulation exerts a torque on the magnetization of the Fe film and can be viewed as a time varying interfacial magnetic field \mathbf{h}_{SO} , which excites the magnetization dynamics. The precessing magnetization causes a resistance variation $R(t)$ via the AMR of Fe. Due to mixing of the alternating current and the oscillating resistance, a dc voltage V results²⁸. Thus, by measuring this dc voltage for different crystallographic directions we can quantitatively determine the effective spin-orbit fields at the Fe/GaAs interface.

The sample used in our study is a 5-nm thick single crystalline Fe film grown by molecular-beam epitaxy (MBE; see Fig. 1c and Methods) on top of a 100 nm thick undoped GaAs buffer layer on a semi-insulating GaAs (001) substrate. Additionally, we grew a polycrystalline Fe reference film on an amorphous SiO_x substrate. Devices of size, $6.4 \times 100.0 \mu\text{m}$, oriented along different crystallographic directions, are defined by employing electron-beam lithography and ion beam etching. Figure 2c shows a typical V trace (where an offset voltage V_{offset} due to thermo-electric effect, has been subtracted) of a [100]-orientated stripe measured at room temperature. To fit the characteristic line shape, we introduce a symmetric ($L_{\text{sym}} = \Delta H^2/[4(H - H_R)^2 + \Delta H^2]$) and an anti-symmetric Lorentzian ($L_{\text{a-sym}} = -4\Delta H(H - H_R)/[4(H - H_R)^2 + \Delta H^2]$), where H_R is the magnetic field H at FMR, ΔH the line width (full width at half maximum: FWHM). $V - V_{\text{offset}}$ is fitted by a combination of L_{sym} and $L_{\text{a-sym}}$, $V_{\text{sym}}L_{\text{sym}} + V_{\text{a-sym}}L_{\text{a-sym}}$, with V_{sym} ($V_{\text{a-sym}}$) the magnitude of the symmetric (anti-symmetric) component of the dc voltage. By fitting we obtain values for H_R , ΔH , V_{sym} and $V_{\text{a-sym}}$. These

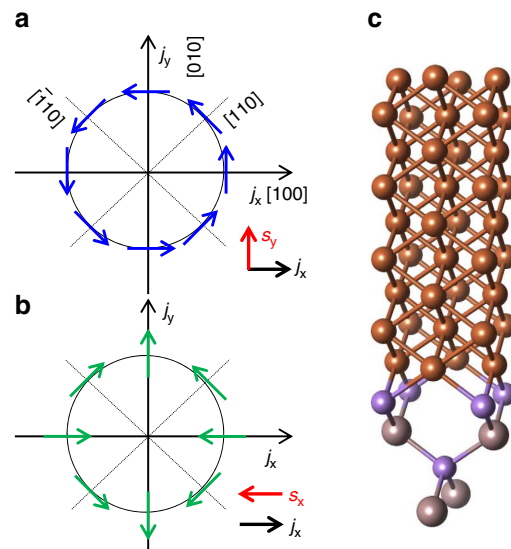


Figure 1 | Spin-orbit coupling at the Fe/GaAs interface. Schematic of Rashba (a) Dresselhaus (b) spin-orbit fields (SOFs) for different crystallographic orientations. Red arrows in a,b denote the direction of spin accumulation induced by a current flow j_x . (c) Atomic structure of the Fe/GaAs (001) spin-orbit interface. Zincblende GaAs exhibits bulk inversion asymmetry (BIA) with D_{2d} symmetry and adding a single crystalline Fe on top of GaAs further lowers the D_{2d} symmetry to C_{2v} . The C_{2v} symmetry results in the Rashba and Dresselhaus SOFs at the Fe/GaAs (001) interface.

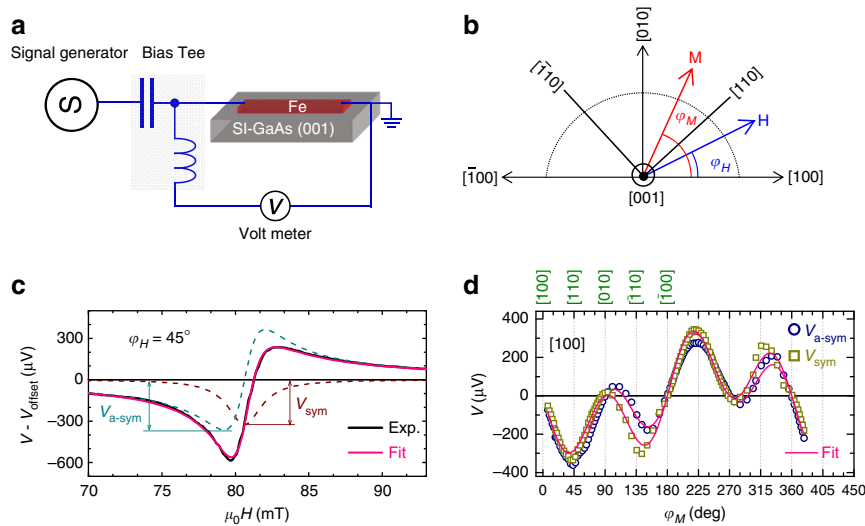


Figure 2 | Spin-orbit ferromagnetic resonance measurements. (a) Depiction of sample structure and experimental set-up. A microwave current passes through the Bias Tee and to the sample to drive the magnetization dynamics in the Fe film. A rectified dc voltage is detected across the Fe stripe. (b) Definition of magnetic-field angle φ_H and magnetization angle φ_M . (c) Typical spectrum of the dc voltage V obtained at a magnetic-field angle of $\varphi_H=45^\circ$, microwaves frequency of 12 GHz, and temperature of 300 K, where the offset voltage V_{offset} is subtracted. (d) Dependence of $V_{\text{a-sym}}$ and V_{sym} on the magnetization angle φ_M for a [100]-orientated device. The solid lines are fits to equation (1).

parameters have been extracted as a function of φ_H and for Fe stripes along different crystallographic directions (see Supplementary Figs 3 and 5). The φ_H -dependence of H_R and ΔH can be well explained by conventional FMR analysis^{29,30}, from which we obtain the Landé g factor ($g=2.12$), the effective demagnetization field ($\mu_0 H_K=1,750$ mT), the biaxial magnetic anisotropy field ($\mu_0 H_B=40$ mT), the uniaxial magnetic anisotropy field ($\mu_0 H_U=48$ mT), and the damping constant ($\alpha=0.0036$) (see Supplementary Note 3).

For comparison, we also tried to measure dc voltages on polycrystalline Fe films deposited on thermally oxidized Si substrates; however, no characteristic dc voltages can be observed at FMR using the same excitation conditions as for single crystalline films of Fe/GaAs, indicating that the driving force for magnetization dynamics originates from the eSOFs at the interface of single crystalline Fe/GaAs and not from any current induced Oersted field (see Supplementary Note 1).

To quantify the magnitude of the eSOFs, it is necessary to understand the dependence of the dc voltage on φ_M . By taking a [100]-orientated stripe as an example, the anti-symmetric and symmetric components can be expressed as (for the derivation of other orientations see Supplementary Note 2 and 3)

$$\begin{aligned} V_{\text{a-sym}}^{[100]} &= -\frac{\Delta\rho jl}{2M} \left(-h^{[100]} \sin \varphi_M + h^{[010]} \cos \varphi_M \right) \text{Re}(\chi^l) \sin 2\varphi_M, \\ V_{\text{sym}}^{[100]} &= \frac{\Delta\rho jl}{2M} h^{[001]} \text{Im}(\chi_a^0) \sin 2\varphi_M, \end{aligned} \quad (1)$$

where $h^{[100]}$, $h^{[010]}$, $h^{[001]}$ are the eSOFs along the [100], [010] and [001] directions, $\Delta\rho$ is the magnitude of AMR, j the microwave current density, l the length of the device, M the magnetization of the Fe film, $\text{Im}(\chi_a^0)$ the imaginary part of the off-diagonal component of the magnetic susceptibility due to out-of-plane excitation ($h^{[001]}$), and $\text{Re}(\chi^l)$ the real part of the diagonal component due to in-plane excitation ($h^{[100]}$ and $h^{[010]}$). Since the dc voltage is induced by FMR, the magnitude of $\text{Im}(\chi_a^0)$ and $\text{Re}(\chi^l)$ can be calculated by solving the Landau-Lifshits-Gilbert equation³¹, which is anisotropic due to the in-plane

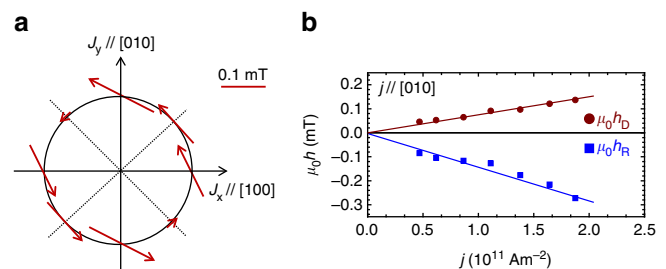


Figure 3 | In-plane spin-orbit fields. (a) Experimentally determined magnitude and direction of the in-plane spin-orbit fields, which are normalized by a unit current density of 10^{11} Am^{-2} . (b) Current density dependence of the magnitudes of $\mu_0 h_R$ and $\mu_0 h_D$ obtained from a [010]-orientated device. From the slope of $\mu_0 h_R$ and $\mu_0 h_D$, the ratio of α and β , $(\alpha/\beta)_{\text{in-plane}}$, is determined to ~ 2.0 .

magnetic anisotropy as well as the angular variation of the linewidth³⁰ (see Supplementary Note 3).

In-plane effective spin-orbit fields. Figure 2d shows the dependence of $V_{\text{a-sym}}$ on the magnetization angle φ_M for the stripes oriented along the [100] direction. The results can be fitted by a superposition of $\sin 2\varphi_M \sin \varphi_M$ and $\sin 2\varphi_M \cos \varphi_M$, indicating that the driving field contains both Dresselhaus and Bychkov-Rashba contributions (see equation (1)). The magnitude of $\mu_0 h^{[100]}$ (Dresselhaus) and $\mu_0 h^{[010]}$ (Bychkov-Rashba) is determined to be -0.15 and 0.28 mT by using $\mu_0 M=1.63$ T, $\Delta\rho=7.0 \times 10^{-10} \Omega\text{m}$, $l=100.0 \mu\text{m}$ and $j=1.91 \times 10^{11} \text{ Am}^{-2}$. Here M and $\Delta\rho$ have been determined by separate magnetization and dc transport measurements, and the microwave current j is calibrated by thermally shifting the resonance field (see Supplementary Note 5).

For an independent crosscheck, we also show in the Supplementary Note 7 that the Dresselhaus field can be alternatively verified by varying H_R via a dc current.

In Fig. 3a, we show direction and magnitude of the in-plane effective spin-orbit fields obtained for a current density of

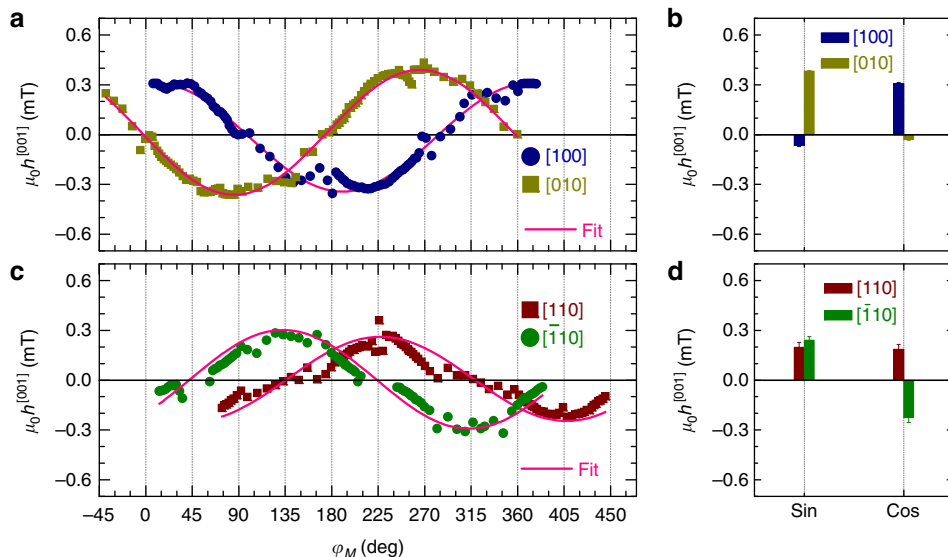


Figure 4 | Out-of-plane spin-orbit fields. (a) Magnetization angle ϕ_M dependences of the out-of-plane spin-orbit field $\mu_0 h^{[001]}$ for [100] and [010]-orientated devices; the solid lines are fits by equation (2), from which $(\alpha/\beta)_{\text{out-of-plane}}$ is obtained (see Supplementary Note 8). The fitting coefficients of $\sin\phi_M$ and $\cos\phi_M$ are shown in (b). (c) ϕ_M dependences of $\mu_0 h_z$ for [110] and [−110] orientated devices. (d) Fitting coefficients of $\sin\phi_M$ and $\cos\phi_M$. The error bar in b,d is the s.d. obtained from the fit. All the fields are normalized by a unit current density of 10^{11} Am^{-2} .

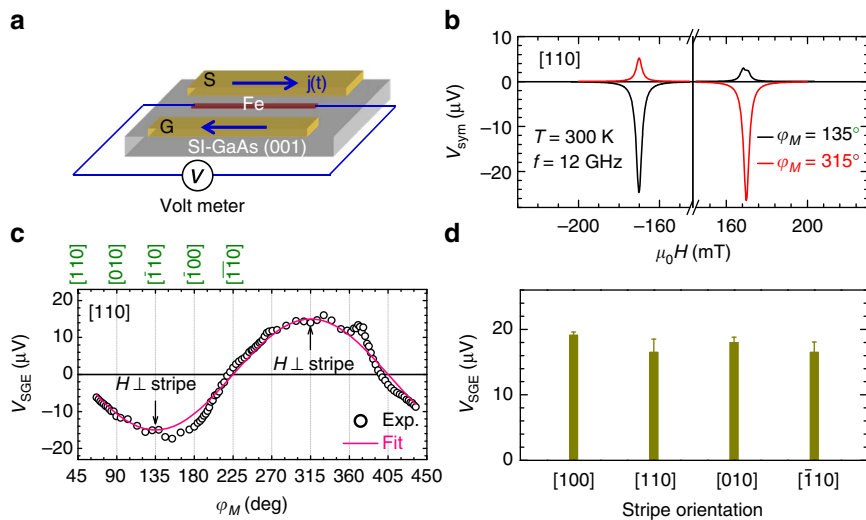


Figure 5 | Spin-galvanic effect in Fe/GaAs. (a) Schematic of the device for spin pumping and spin-galvanic effect SGE. The [110]-orientated Fe/GaAs stripe is integrated between the signal (S) and ground (G) lines of the coplanar waveguide (CPW). (b) Magnetic-field $\mu_0 H$ dependent voltage measured at 300 K for $\phi_M = 135^\circ$ and 315° . This is the ideal configuration for the study of SGE since the parasitic AMR of Fe is absent when H is perpendicular to the stripe. (c) Magnetization angle ϕ_M dependence of V_{SGE} , the solid line is a fit to $\cos(\phi_M + 45^\circ)$. (d) Crystallographic orientation dependence of the magnitude of V_{SGE} . The error bar is the s.d. obtained by fitting the ϕ_M dependence of V_{SGE} for different stripe orientations.

10^{11} Am^{-2} in a polar plot for devices with different orientations. Figure 3a indicates that Bychkov-Rashba is the dominating contribution since the field vectors along [100] and [010] directions align mainly perpendicular to the current direction. For [110] and [−110] directions, the spin-orbit fields are perpendicular to the current as expected for both Rashba and Dresselhaus contribution (Fig. 1a,b). Although the current induced Oersted field may also cause a field contribution perpendicular to the current directions, this effect is expected to be small for two reasons: First, the magnitude of the SOF for the [−110] direction is ~ 5 times smaller than that for the [110] direction for a similar current density (Fig. 3a and Supplementary Fig. 5b), which indicates that the effect is intrinsically related to SOI. Second, the non-detectable dc voltage in Fe/SiO_x further excludes a sizeable influence of any Oersted field. The different

magnitudes of the eSOFs along the [110] and [−110] directions stem from constructive and destructive superposition of Dresselhaus and Bychkov-Rashba fields (see Fig. 1a,b). In Fig. 3b, we show that the amplitudes of $\mu_0 h_R$ and $\mu_0 h_D$ in the [010] stripe increase linearly with the current density, indicating that reduction of M and $\Delta\rho$ due to Joule heating is negligibly small in the device. From the slope of h_R and h_D , the ratio of α and β , $(\alpha/\beta)_{\text{in-plane}}$, is determined to be ~ 2 . We have repeated these measurements for two more sets of devices (eight devices); each set shows similar behaviour.

Out-of-plane effective spin-orbit fields. The presence of the component V_{sym} displayed in Fig. 2c implies a sizeable out-of-plane effective spin-orbit field (see equation (1)). Figure 2d shows

the dependence of V_{sym} on φ_M for a current flowing along the [100] direction. The results cannot simply be fitted by $\sin 2\varphi_M$ indicating that $h^{[001]}$ depends on φ_M . Figure 4a,c show the φ_M dependence of $h^{[001]}$ for four crystallographic orientations. Here one can see that $h^{[001]}$ strongly depends on φ_M and reaches a value as large as 0.35 mT for a current density of 10^{11} Am^{-2} . We estimate that the magnitude of the SOT in our system is comparable to that observed in ferromagnetic metal/non-magnetic metal bi-layer systems^{19–22} (see Supplementary Note 9). Note that an additional contribution to the symmetric part of the dc voltage can in principle arise from spin pumping together with the spin galvanic effect. However, we calculate that this effect is two orders of magnitude smaller than the detected spin-orbit voltage.

To gain insight into the microscopic origin of the interfacial out-of-plane spin-orbit field, we show in Supplementary Note 8 that, within a two-dimensional spin-orbit ferromagnet model³², $h^{[001]}$ is given by

$$\mu_0 h^{[001]} = [e/(2\mu_B h_{\text{ex}})] \left[\alpha \left(\cos \varphi_M E^{[100]} + \sin \varphi_M E^{[010]} \right) - \beta \left(\cos \varphi_M E^{[010]} + \sin \varphi_M E^{[100]} \right) \right], \quad (2)$$

where $E^{[100]}$, $E^{[010]}$ is the electric field along the [100] and [010] directions, e the electronic charge, μ_B the Bohr magneton, and h_{ex} the exchange field. First, we estimate from this equation that the expected magnitude of $h^{[001]}$ agrees well with the experiment (Supplementary Note 8). According to equation (2), the φ_M dependence of $h^{[001]}$ can be explained by a combination of $\sin \varphi_M$ and $\cos \varphi_M$ terms depending on the symmetry of the SOI. The fitting coefficients of the $\sin \varphi_M$ and $\cos \varphi_M$ terms are shown in Fig. 4b,d (Supplementary Note 8). For the [100] and [010] directions, the $\cos \varphi_M$ and $\sin \varphi_M$ terms dominate, respectively. This indicates again that the Bychkov-Rashba SOI is the dominating SOI at the Fe/GaAs interface¹³. Moreover, the fitting coefficients for [110] and [−110] directions also agree well with the theoretical model of Bychkov-Rashba dominated SOI. From the fitting coefficients, the ratio of α and β , $(\alpha/\beta)_{\text{out-of-plane}}$ is determined. The value of $(\alpha/\beta)_{\text{out-of-plane}}$ for each device is larger than that of $(\alpha/\beta)_{\text{in-plane}}$ (see Supplementary Note 8). This is due to the different origins between in-plane and out-of-plane induced spin polarization. The in-plane spin polarization is created only at the Fermi level, while the out-of-plane spin polarization is due to the electrical polarization (intrinsic effect) of the whole bands³². Previous work on the ferromagnetic semiconductor (Ga,Mn)As^{13,33} explains an emerging $h^{[001]}$ by the Kubo formalism, taking into account the presence of Dresselhaus dominated SOI and p - d exchange coupling. However, for our system of Fe/GaAs, $h^{[001]}$ results from the broken symmetry at the interface and interfacial exchange coupling, a scenario which is distinctly different from the (Ga,Mn)As case.

Measurement of the SGE. The effective spin-orbit fields stem from charge-to-spin conversion. In the following we demonstrate the inverse process, i.e., spin-to-charge conversion. In ferromagnetic metal/non-magnetic bilayers, spin pumping generates pure spin currents in the ferromagnetic layer. The pure spin current flows within the spin diffusion length into the non-magnetic layer and generates a transverse electrical current due to SOI, which is called ISHE^{23–25}.

Figure 5a shows the schematic of the device used in our experiments. Fe/GaAs stripes with different orientations are integrated in the gap between the signal line and the ground plane of a coplanar waveguide. The stripe experiences an out-of-plane Oersted field excitation, which has been demonstrated to be an

ideal configuration to study spin pumping and ISHE^{34,35}. Figure 5b shows the measured voltage when the external magnetic field is in the plane but perpendicular to the stripe. For $\varphi_M = 135^\circ$, the voltage has the opposite polarity at $\pm H_R$ but differs in magnitude, $|V(-H_R)| > |V(+H_R)|$. When the external magnetic field is rotated by 180° , the polarity reverses and $|V(-H_R)| < |V(+H_R)|$ holds. This behaviour³⁶ evidences the ISHE in ferromagnetic/non-magnetic layers and, in our case without the non-magnetic conducting layer, the presence of the SGE. The difference in the absolute magnitude at $\pm H_R$ indicates that a symmetric thermo-electric background³⁷ coexists with the SGE, so that the magnitude of the spin-galvanic voltage V_{SGE} can be obtained by $V_{\text{SGE}} = [V(-H_R) - V(H_R)]/2$ (see Supplementary Note 10). The φ_M dependence of V_{SGE} , presented in Fig. 5c, can be fitted by $\cos(\varphi_M + 45^\circ)$, concordant with the SGE⁶. Due to the C_{2v} symmetry of the system, the electric current flows always perpendicular to the spin polarization (magnetization)⁶. The angular dependence suggests that the Rashba SOI dominates the spin-to-charge conversion process. As shown in Fig. 5d, the SGE occurs in each orientations and the magnitude of V_{SGE} takes similar values for different orientations, indicating a similar strength of the Rashba SOI. An anisotropy in V_{SGE} could, in principle, be expected due to anisotropic scattering. However, according to the measurements of anisotropic tunnelling magnetoresistance¹⁷ and crystalline AMR¹⁸, the anisotropy is smaller than 1%. This should also be case for V_{SGE} , which is beyond our detection limit.

Discussion

We notice that in our system consisting of single crystalline Fe/GaAs, it is difficult to determine the magnitude of the spin current J_S injected into the interface by comparing the damping enhancement as commonly done for ferromagnetic/non-magnetic bilayers^{38,39} (for example, for Py/Pt bilayers, the damping constant is usually compared with that of Py/SiO_x). The enhancement of damping is used to determine the spin mixing conductance and then J_S). Recent experiments²⁶ and microscopic theory⁴⁰ suggest that the magnitude of J_S can be estimated by $J_S = J_C / \lambda_{\text{SGE}}$, where $J_C = I_C / w$ (I_C is the charge current density and w the width of the stripe) is an areal current density and λ_{SGE} the ‘effective thickness’ of the spin-orbit layer. Our previous magneto-transport measurements¹⁸ show that the symmetry of AMR changes when the Fe layer reaches a characteristic thickness of ~ 4 monolayers (0.57 nm). This is evidence for the presence of interfacial SOFs, which gives an upper limit of λ_{SGE} . By using an average J_C of $6.7 \times 10^{-4} \text{ Am}^{-1}$, the lower bound of J_S is determined to be $1.2 \times 10^6 \text{ Am}^{-2}$. This value is in good agreement with that in ferromagnetic/non-magnetic bilayers^{26,34,41} for a similar excitation. It should also be noted that at the Fe/GaAs interface both ferromagnetic exchange exists and SOI emerges. The generation of pure spin currents by spin pumping is due to the Fe exchange interaction and the spin-to-charge conversion occurs at the interfacial Fe layer due to SOI. The whole process occurs in one system. This is significantly different from any ferromagnet/non-magnetic bi-layer ever studied^{25–27,30,34–39,41}, where the ferromagnetic and non-magnetic layer is separated and decoupled.

In summary, we have observed mutual conversion between charge and spin current, which is known as the SGE and inverse SGE, at an epitaxial Fe/GaAs interface by SO-FMR and spin pumping at room temperature. The magnitudes of the interfacial SOT in this single crystalline ferromagnetic metal/semiconductor system are found to be comparable to those at ferromagnetic metal/non-magnetic metal interfaces, which could be useful for future spintronic applications. Our findings open a pathway in

search for efficient SOT in various single crystalline ferromagnetic metal/semiconductor interfaces.

Methods

Sample preparation. To guarantee high quality of the interfaces, Fe/GaAs samples are grown by MBE in a MBE cluster with *in-situ* transfer. First, an undoped GaAs buffer layer (100 nm) is deposited on top of a GaAs (001) semi-insulating substrate at 560 °C. Clear (2 × 4) surface construction pattern has been observed, indicating an As-terminated flat surface. Then, without breaking the vacuum, the sample is transferred to another MBE chamber, where a 5-nm Fe film is deposited on GaAs at a substrate temperature of 75 °C. Reflection high-energy electron diffraction oscillations have been observed during growth, indicating the epitaxial growth mode as well as the flat interface between Fe/GaAs. Finally, a 3-nm thick Al capping layer is deposited onto the Fe film to avoid oxidation. The high quality of the Fe films is evidenced by the small damping constant of 0.0036 (see Supplementary Note 3).

Device. For the SO-FMR measurements, $6.4 \times 100.0\text{ }\mu\text{m}$ stripes with different orientations are defined by electron-beam lithography and ion beam etching. The contacts are made from 15 nm Ti and 150 nm Au. All stripes have a resistance of $\sim 1.6\text{ k}\Omega$. For spin pumping measurements, $10.0 \times 400.0\text{ }\mu\text{m}$ stripes with different orientations are integrated in the gap of the signal and ground lines of a coplanar wave guide. The resistances of the stripes are $\sim 2.6\text{ k}\Omega$. The width of the signal and ground line, which are also made from 15 nm Ti and 150 nm Au, is 50 and $30\text{ }\mu\text{m}$, respectively.

Measurements. For both SO-FMR and spin pumping measurements, microwave currents with a frequency of 12 GHz are used and the input microwave power is 22 dBm ($\sim 158\text{ mW}$). For SO-FMR measurements, a Bias Tee is used to separate the dc voltage from microwave background, and the driving power acting on the sample is estimated to be 65 mW. Since the skin depth at 12 GHz ($\sim 145\text{ nm}$) is much larger than the Fe thickness (5 nm), the current density in Fe is expected to be spatially uniform. Thus, the Oersted field should not produce torque on Fe itself. All measurements are performed at room temperature.

Data availability. The data that support the findings of this study are available from the corresponding author on request.

References

- Dresselhaus, G. Spin-orbit coupling effects in zincblende structures. *Phys. Rev.* **100**, 580–586 (1955).
- Bychkov, Y. A. & Rashba, E. I. Oscillatory effects and the magnetic susceptibility of carriers in inversion layers. *J. Phys. C: Solid State Phys.* **17**, 6039–6045 (1984).
- Aronov, A. G., Lyanda-Geller, Y. B. & Pikus, G. E. Spin polarization of electrons by an electric current. *Sov. Phys. JETP* **73**, 537–541 (1991).
- Edelstein, V. M. Spin polarization of conduction electrons induced by electric current in two-dimensional asymmetric electron systems. *Solid State Commun.* **73**, 233–235 (1990).
- Sinova, J. *et al.* Universal intrinsic spin Hall effect. *Phys. Rev. Lett.* **92**, 126603 (2004).
- Ganichev, S. D. *et al.* Spin-galvanic effect. *Nature* **417**, 153–156 (2002).
- Sinova, J., Valenzuela, S. O., Wunderlich, J., Back, C. H. & Jungwirth, T. Spin Hall effects. *Rev. Mod. Phys.* **87**, 1213–1259 (2015).
- Miron, I. M. *et al.* Perpendicular switching of a single ferromagnetic layer induced by in-plane current injection. *Nature* **476**, 189–193 (2011).
- Liu, L. Q. *et al.* Spin-torque switching with the giant spin Hall effect of Tantalum. *Science* **336**, 555–558 (2012).
- Chernyshov, A. *et al.* Evidence for reversible control of magnetization in a ferromagnetic material by means of spin-orbit magnetic field. *Nat. Phys.* **5**, 656–659 (2009).
- Endo, M., Matsukura, F. & Ohno, H. Current induced effective magnetic field and magnetization reversal in uniaxial anisotropy (Ga,Mn)As. *Appl. Phys. Lett.* **97**, 222501 (2010).
- Fang, D. *et al.* Spin-orbit-driven ferromagnetic resonance. *Nat. Nanotech.* **6**, 413–417 (2011).
- Kurebayashi, H. *et al.* An antidamping spin-orbit torque originating from the Berry curvature. *Nat. Nanotech.* **9**, 211–217 (2014).
- Ciccarelli, C. *et al.* Room-temperature spin-orbit torque in NiMnSb. *Nat. Phys.* **12**, 855–860 (2016).
- Wadley, P. *et al.* Electrical switching of an antiferromagnet. *Science* **351**, 587–590 (2016).
- Gmitra, M., Matos-Abiague, A., Draxl, C. & Fabian, J. Magnetic control of spin-orbit fields: a first-principle study of Fe/GaAs junctions. *Phys. Rev. Lett.* **111**, 036603 (2013).
- Moser, J. *et al.* Tunneling anisotropic magnetoresistance and spin-orbit coupling in Fe/GaAs/Au tunnel junctions. *Phys. Rev. Lett.* **99**, 056601 (2007).
- Hupfauer, T. *et al.* Emergence of spin-orbit fields in magnetotransport of quasi-two-dimensional iron on gallium arsenide. *Nat. Commun.* **6**, 7374 (2015).
- Garello, K. *et al.* Symmetry and magnitude of spin-orbit torques in ferromagnetic heterostructures. *Nat. Nanotech.* **8**, 587–593 (2013).
- Fan, X. *et al.* Quantifying interface and bulk contributions to spin-orbit torque in magnetic bilayers. *Nat. Commun.* **5**, 3042 (2014).
- Kim, J. *et al.* Layer thickness dependence of the current-induced effective field vector in Ta [CoFeB] MgO. *Nat. Mater.* **12**, 240–245 (2013).
- Skinner, T. D. *et al.* Complementary spin-Hall and inverse spin-galvanic effect torques in a ferromagnet/semiconductor bilayer. *Nat. Commun.* **6**, 6730 (2015).
- Tserkovyak, Y. *et al.* Enhanced Gilbert damping in thin ferromagnetic films. *Phys. Rev. Lett.* **88**, 117601 (2002).
- Mizukami, S., Ando, Y. & Miyazaki, T. Effect of spin diffusion on Gilbert damping for a very thin permalloy layer in Cu/permalloy/Cu/Pt films. *Phys. Rev. B* **66**, 104413 (2002).
- Saitoh, E., Ueda, M., Miyajima, H. & Tatara, G. Conversion of spin current into charge current at room temperature: inverse spin-Hall effect. *Appl. Phys. Lett.* **88**, 182509 (2006).
- Rojas-Sánchez, J. C. *et al.* Spin-to-charge conversion using Rashba coupling at the interface between non-magnetic materials. *Nat. Commun.* **4**, 2944 (2013).
- Rinaldi, C. *et al.* Evidence for spin to charge conversion in GeTe(111). *APL Mater.* **4**, 032501 (2016).
- Juretschke, H. J. Electromagnetic theory of dc effects in ferromagnetic resonance. *J. Appl. Phys.* **31**, 1401–1406 (1960).
- Liu, X. & Furdyna, J. K. Ferromagnetic resonance in $\text{Ga}_{1-x}\text{Mn}_x\text{As}$ dilute magnetic semiconductors. *J. Phys. Condens. Matter* **18**, R245–R279 (2006).
- Chen, L., Matsukura, F. & Ohno, H. Direct-current voltages in (Ga,Mn)As structures induced by ferromagnetic resonance. *Nat. Commun.* **4**, 2055 (2013).
- Gilbert, T. L. A phenomenological theory of damping in ferromagnetic materials. *IEEE Trans. Magn.* **40**, 3443–3449 (2004).
- Qaiumzadeh, A., Duine, R. A. & Titov, M. Spin-orbit torques in two-dimensional Rashba ferromagnets. *Phys. Rev. B* **92**, 014402 (2015).
- Li, H. *et al.* Intraband and interband spin-orbit torques in noncentrosymmetric ferromagnets. *Phys. Rev. B* **91**, 134403 (2015).
- Obstbaum, M. *et al.* Inverse spin Hall effect in $\text{Ni}_{81}\text{Fe}_{19}$ /normal-metal bilayers. *Phys. Rev. B* **89**, 060407 (R) (2014).
- Bai, L. H., Feng, Z., Hyde, P., Ding, H. F. & Hu, C. M. Distinguishing spin pumping from spin rectification in a Pt/Py bilayer through angle dependence line shape analysis. *Appl. Phys. Lett.* **102**, 242402 (2013).
- Bai, L. H. *et al.* Universal method for separating spin pumping from spin rectification voltage of ferromagnetic resonance. *Phys. Rev. Lett.* **111**, 217602 (2013).
- Shiochi, Y. *et al.* Spin-electricity conversion induced by spin injection into topological insulators. *Phys. Rev. Lett.* **113**, 196601 (2014).
- Urban, R., Woltersdorf, G. & Heinrich, B. Gilbert damping in single and multilayer ultrathin films: Role of interfaces in nonlocal spin dynamics. *Phys. Rev. Lett.* **87**, 217204 (2001).
- Mosendz, O. *et al.* Quantifying spin Hall angles from spin pumping: experiments and theory. *Phys. Rev. Lett.* **104**, 046601 (2010).
- Shen, K., Vignale, G. & Raimondi, R. Microscopic theory of the inverse Edelstein effect. *Phys. Rev. Lett.* **112**, 096601 (2014).
- Wei, D. H., Obstbaum, M., Ribow, M., Back, C. H. & Woltersdorf, G. Spin Hall voltages from a.c. and d.c. spin currents. *Nat. Commun.* **5**, 3768 (2014).

Acknowledgements

L.C. is grateful for the support from Alexander von Humboldt Foundation. This work is supported by the German Science Foundation (DFG) via SFB 689 and SPP 1538.

Author contributions

L.C., C.H.B and D.W. planned the study and wrote the manuscript. M.K., D.S., D.B. did the MBE growth; L.C., R.I. and M.D. fabricated the devices. L.C. collected and analysed the experimental data. J.F. and M.G. developed the theory. All authors discussed the results.

Additional information

Supplementary Information accompanies this paper at <http://www.nature.com/naturecommunications>

Competing financial interests: The authors declare no competing financial interests.

Reprints and permission information is available online at <http://npg.nature.com/reprintsandpermissions/>

How to cite this article: Chen, L. *et al.* Robust spin-orbit torque and spin-galvanic effect at the Fe/GaAs (001) interface at room temperature. *Nat. Commun.* 7, 13802 doi: 10.1038/ncomms13802 (2016).

Publisher's note: Springer Nature remains neutral with regard to jurisdictional claims in published maps and institutional affiliations.



This work is licensed under a Creative Commons Attribution 4.0 International License. The images or other third party material in this article are included in the article's Creative Commons license, unless indicated otherwise in the credit line; if the material is not included under the Creative Commons license, users will need to obtain permission from the license holder to reproduce the material. To view a copy of this license, visit <http://creativecommons.org/licenses/by/4.0/>

© The Author(s) 2016